European Radiology (2019) 29:1778–1786
https://doi.org/10.1007/s00330-018-5708-4

BREAST

Diagnostic value of electric properties tomography (EPT) for differentiating benign from malignant breast lesions: comparison with standard dynamic contrast-enhanced MRI

Naoko Mori[1,2] · Keiko Tsuchiya[3] · Deepa Sheth[1] · Shunji Mugikura[2] · Kei Takase[2] · Ulrich Katscher[4] · Hiroyuki Abe[1]

Received: 9 April 2018 / Revised: 17 July 2018 / Accepted: 6 August 2018 / Published online: 25 September 2018

Abstract

Objectives To evaluate the diagnostic utility of electric properties tomography (EPT) in differentiating benign from malignant breast lesions in comparison with dynamic contrast-enhanced magnetic resonance imaging (DCE-MRI).

Methods In this institutional review board-approved retrospective study, 116 consecutive patients with 141 breast lesions (50 benign and 91 malignant) underwent 3-T MRI, including 3D turbo-spin echo (TSE) sequence and standard DCE-MRI scans between January 2014 and January 2017. The lesions were segmented semi-automatically using subtraction DCE-MR images, and they were registered to the phase images from 3D TSE. The mean conductivity of the lesion was obtained from phase-based reconstruction of lesions. From the DCE-MRI, initial enhancement rate (IER) and signal enhancement ratio (SER) were calculated from signal intensity (SI) as follows: IER = (SI_{early} - SI_{pre})/SI_{pre}, SER = (SI_{early} - SI_{pre})/($SI_{delayed}$ - SI_{pre}). The parameters from EPT and the DCE-MRI were compared between benign and malignant lesions.

Results There was significant difference in mean conductivity (0.14 ± 1.77 vs 1.14 ± 1.36 S/m, $p < 0.0001$) and SER (0.77 ± 0.28 vs 1.04 ± 0.25, $p < 0.0001$) between benign and malignant lesions, but not in IER ($p = 0.06$). Receiver operating curve (ROC) analysis revealed that the area under the curve (AUC) of the mean conductivity and SER was 0.71 and 0.80, respectively, without significant difference ($p = 0.15$).

Conclusions The mean conductivity of EPT was significantly different between benign and malignant breast lesions as well as kinetic parameter or SER from DCE-MRI.

Key Points

- *The conductivity of malignant lesions was higher than that of benign lesions.*
- *EPT helps differentiatie benign from malignant lesions.*
- *Diagnostic ability of EPT was not significantly different from that of DCE-MRI.*

Keywords Electric conductivity · Magnetic resonance imaging · Breast cancer

Electronic supplementary material The online version of this article (https://doi.org/10.1007/s00330-018-5708-4) contains supplementary material, which is available to authorized users.

✉ Naoko Mori
naokomori7127@gmail.com

[1] Department of Radiology, The University of Chicago, 5841 S Maryland Ave, MC 2026, Chicago, IL 60637, USA

[2] Department of Diagnostic Radiology, Tohoku University Graduate School of Medicine, Seiryo 1-1, Sendai 980-8574, Japan

[3] Department of Radiology, Shiga University of Medical Science, Setatsukinowa-cho, Otsu, Shiga, Japan

[4] Philips Technologie GmbH, Research Laboratories, Roentgenstraße 24-26, 22335 Hamburg, Germany

Abbreviations

DCE-MRI	Dynamic contrast-enhanced magnetic resonance imaging
EPT	Electric properties tomography
FGT	Fibrograndular tissue
IER	Initial enhancement rate
SER	Signal enhancement ratio
T2-VISTA	T2-volume isotropic turbo spin echo acquisition
TSC	Tissue sodium concentration

Introduction

Breast magnetic resonance imaging (MRI) is well established in clinical practice with high sensitivity and reasonable specificity in differentiating benign and malignant lesions [1–5]. According to the BI-RADS lexicon [6], morphological analysis and kinetic curve assessment of dynamic contrast-enhanced MRI (DCE-MRI) are the two most important methods in the clinical interpretation of breast lesions.

Gadolinium diethylene triamine penta-acetic acid (Gd-DTPA), a widely used MR contrast medium, distributes in the extracellular space after intravenous injection and accumulates in tissues with rich vascularity or an expanded interstitial space [7, 8]. This mechanism of distribution allows for the differentiation between benign and malignant vasculature using the enhancement effect [9, 10]. Emerging evidence that gadolinium deposits in deep nuclei of the brain has become a concern for patient safety [11, 12], although its clinical significance is not fully understood. Thus, novel techniques that do not require gadolinium contrast media to differentiate malignant from benign breast lesions would potentially have great merit.

Electric properties tomography (EPT) is a novel technique using MRI to investigate the conductivity of a lesion [13]. The conductivity can be obtained from a basic clinical sequence without contrast injection [i.e. turbo-spin echo (TSE)]. The factors that lead to elevated conductivity in malignant tumours include: increased tissue sodium concentration (TSC) and concentration of additional ions such as potassium or calcium, and changes in water content. TSC was reported as a potential major determinant of electric tissue conductivity [14–16]. TSC is increased as a result of altered Na^+ and H^+ transport kinetics and pH levels in proliferating cells [17]. Several studies showed significantly higher TSC in malignant tumours than in normal tissue in the brain and in the breast [14, 18, 19]. Because the conductivity measured by EPT is largely influenced by TSC [16], EPT might be a possible candidate for a non-contrast tissue biomarker.

Several studies have shown that the conductivity of a brain tumour is higher than that of surrounding normal white matter [20–22]. With regards to the breast, recent studies have reported a relationship between the conductivity and breast tumours [23, 24]. Shin et al [23] reported that malignant lesions showed significantly increased conductivity compared to benign lesions; however, their study included a limited number of subjects; only 5 benign and 30 malignant subjects. More reliable results should be obtained with a larger number of subjects, particularly benign subjects, in order to confirm the utility of conductivity to differentiate benign from malignant lesions. Furthermore, there have been no studies, to our knowledge, comparing EPT with that of standard DCE-MRI in terms of differentiating between benign and malignant lesions.

The purpose of this study was to evaluate the diagnostic ability of EPT in differentiating between benign and malignant breast lesions in comparison with conventional parameters of DCE-MRI.

Materials and methods

Patients

Our institutional review board approved this retrospective study and waived the informed consent requirement. We retrospectively reviewed breast MRI studies performed at our institution between January 2014 and January 2017. Among patients who underwent 3-T breast MRI including three-dimensional (3D) TSE or T2-volume isotropic TSE acquisition (T2-VISTA), which is a clinical non-contrast 3D turbo-spin echo (TSE) sequence, 133 consecutive patients had biopsy-proven benign or malignant lesions, or clinically confirmed benign lesions. The following patients were excluded:

1. Six patients with a too small lesion (less than $5.6 \times 5.6 \times 11.2$ mm^3: diameter of 7 voxels), and six patients with non-mass enhancement consisting of too small components (less than $5.6 \times 5.6 \times 11.2$ mm^3). For these patients, calculation of conductivity did not work well because the numerical differentiation according to the equation requires at least 3 voxels in each spatial direction, which together with the safety margin results in a minimal lesion diameter of 7 voxels ($5.6 \times 5.6 \times 11.2$ mm^3) for conductivity reconstruction.
2. Five patients with severe susceptibility artefact because of placement of metallic clips. In our method, the segmentation of target lesions was performed on the subtraction images obtained with T1-weighted gradient echo sequence, and the results of the segmentation were subsequently applied to the phase components of the 3D TSE images. As we used the gradient echo sequence for segmentation, severe susceptibility artefact was inevitable from metallic clips. Although we managed to obtain the conductivity values in majority of the lesions, we had to exclude five lesions, in which the severe metallic artefacts occurred at the centre of the lesion, and the central defect of the segmentation precluded the calculation of conductivity.

Thus, 116 patients with 141 lesions (50 benign and 91 malignant) were included in this retrospective study. The indications of breast MRI for our study population were preoperative staging of known cancer for 56 patients, screening with personal history of breast cancer or strong family history of breast cancer and/or gene mutation for 19 patients, and further evaluation of suspicious breast lesions for 41 patients. All patients were female with mean age of 50 (range, 23–76) years.

The malignant lesions consisted of 73 invasive ductal carcinomas (IDC), 9 ductal carcinomas in situ (DCIS), 7 invasive lobular carcinomas (ILC), 1 invasive micropapillary

carcinoma and 1 metaplastic carcinoma. The benign lesions consisted of 41 with pathologic proof by percutaneous core needle biopsy and 9 lesions diagnosed as benign by follow-up examination of more than 2 years. Forty-one pathologically proven benign lesions were: 24 fibroadenomas, 4 papillomas, 3 apocrine metaplasia, 3 complex sclerosing lesions, 2 chronic periductal inflammation, 1 focal columnar change, 1 lobular carcinoma in situ, 1 extra-abdominal desmoid, 1 hyalinised breast tissue, 1 pseudo-angiomatous stromal hyperplasia (PASH). Remaining 9 benign lesions had been clinically diagnosed as fibroadenoma by >2 years of follow-up with mammogram and/or ultrasound (US).

MRI acquisition

A 3-T system (Achieva 3T-TX system; Philips Healthcare, Best, The Netherlands) with multiple-source radiofrequency transmission was used for all scans. All patients were imaged in the prone position with both breasts placed in a 16-channel bilateral breast coil. Imaging protocol include 3D TSE (T2 VISTA) and DCE-MRI using a 3D fat-suppressed T1-weighted gradient-echo sequence: 3D TSE (T2 VISTA) which routinely includes magnitude and phase images (repetition time/echo time (ms), 2,000/210; matrix, 500 × 500; voxel size, 0.8 × 0.8 × 1.6 mm^3; field of view, 360 mm; NSA, 1; ETL, 120; acceleration factor for parallel imaging, right-left: 3, feet-head: 2; acquisition time, 5 min 10 s), and DCE-MRI (repetition time/echo time (ms), 4.8/2.4; matrix, 500 × 500; voxel size, 0.8 × 0.8 × 1.6 mm^3; field of view, 360 mm; SENSE acceleration factor (RL), 2.5; SENSE acceleration factor (FH), 2; half scan factor, 0.85 (ky): 1 (kz); temporal resolution 65 s; number of sections, 215; flip angle, 10°; fat suppression method, SPAIR). The DCE series consisted of one standard scan before contrast media injection, followed by four standard scans after the injection of gadobentate dimeglumine (Multihance; Bracco, NJ, USA) at a dose of 0.1 mmol/kg and a rate of 2 ml/s, followed by a 20-ml saline flush at a rate of 2 ml/s. The first post-contrast scan (early phase) started at 66 s and ended at 131 s after contrast medium injection, slightly delayed due to the acquisition of research sequences immediately after the injection of contrast medium [25]. The fourth post-contrast scan (delayed phase) started at 261 s and ended at 326 s after contrast medium injection.

Registration and tissue segmentation to avoid conductivity artefacts using DCE-MRI

DICOM data of both 3D TSE and DCE-MR images were transferred to a personal computer and processed using in-house software. First, zoomed images of the target lesion and surrounding parenchyma were obtained from the 3D TSE and DCE-MRI subtraction image (both images were scanned with the same spatial resolution). Then image registration was performed for both of the zoomed images (Fig. 1). Second, 3D segmentation of the target lesion was automatically performed using the DCE-MRI subtraction images (Fig. 1). Segmentation allows for the reduction of conductivity discontinuities which occurs due to a mixed composition of breast glandular tissue and adipose tissue (both of which have vastly differing σ values) [26]. Therefore, image segmentation and individual lesion reconstruction was performed. The signal threshold for segmentation was extracted from the histogram of signal intensities of the voxels in the area of the lesion, separating contrast-enhanced from non-contrast-enhanced regions [27]. Then a binary mask of the lesion was applied to the phase components obtained from the 3D TSE images (Fig. 1).

Phase-based conductivity imaging

MR spin excitation is related to the complex-valued, positive circularly polarised component $B1^+ = |B1^+|\exp(i\varphi^+)$ of the RF field of the transmit coil applied. The magnitude $|B1^+|$ can be measured directly using conventional B1 mapping techniques. The phase φ^+ cannot be measured directly, since the phase of an MR image always contains the superposition of φ^+ with its counterpart φ^- from the negative circularly polarised component $B1^- = |B1^-|\exp(i\varphi^-)$, related to RF reception. This superposition yields the so-called transceive phase $\varphi^{\pm} = \varphi^+ + \varphi^-$. The standard way to estimate φ^+ from $\varphi^{\pm}$ is via the so-called "transceive phase assumption" (TPA) $\varphi^+ \approx \varphi^{\pm}/2$ [28]. This estimation is justified if the magnitude of $B1^+$ is sufficiently constant (at least in the area of the corresponding lesion), which is fulfilled by using the multiple-source radiofrequency transmission of the MR system.

The unknown conductivity σ can be calculated from the measured transceive phase $\varphi^{\pm}$ via the simplified Helmholtz equation (*see* Appendix for derivation of this equation)

$$\sigma \approx \frac{\Delta\varphi^{\pm}}{2\mu_0\omega} \tag{1}$$

where Δ indicates the Laplace operator (i.e. the sum of the second derivative in all three spatial directions), μ_0 indicates the magnetic permeability (assumed to be constant) and ω indicates the Larmor frequency.

To reverse the noise amplification inevitably introduced by the Laplace operator of Eq. (1), a denoising median filter is applied to the conductivity resulting from Eq. (1).

To ensure that boundary artifacts are excluded, a safety margin of two voxels along the lesion's boundary is introduced. The numerical differentiation according to Eq. (1) requires at least 3 voxels in each spatial direction, which together with the mentioned safety margin results in a minimal lesion diameter of 7 voxels (5.6 × 5.6 × 11.2 mm^3) for reconstruction. Lesions below this size cannot be reconstructed

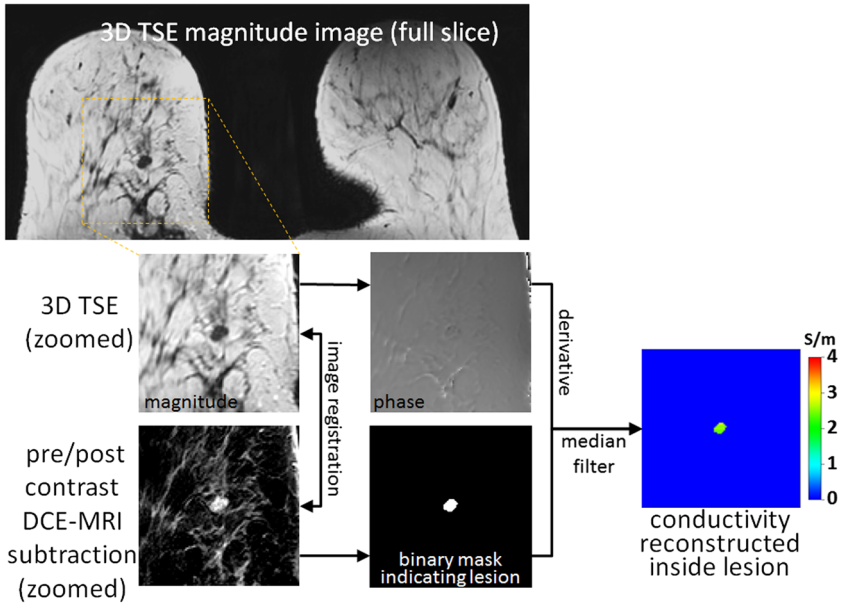

Fig. 1 Flowchart of image processing steps. The zoomed images including a target lesion and surrounding area were obtained from the 3D TSE image and pre/post-contrast DCE-MRI subtraction image, and image registration was performed for both of these zoomed images. Then, a segmentation of a target lesion was performed using the pre/post-contrast DCE-MRI subtraction images to make the binary mask indicating the lesion. The binary mask was applied to the phase images obtained from 3D TSE images. The conductivity was calculated inside the lesion according to Eq. (1) with a denoising median filter. The *bar* on the right side shows the colour scale of conductivity

within this study. Furthermore, non-mass enhancing lesions predominantly consisting of filaments falling below this limit are excluded from this study.

We evaluated the relationship of conductivity to patients' age, amount of fibrograndular tissue (FGT), lesion diameter, lesion appearance (mass or non-mass) and presence/absence of clips (with or without). Then, mean conductivity was compared between benign and malignant lesions.

Analysis of DCE-MRI

The longest lesion diameter and lesion appearance (mass or non-mass) were initially evaluated using DCE-MRI blinded to the clinical and pathological information according to the BI-RADS MRI criteria by consensus of two radiologists (9 and 14 years of experience in breast MRI) [6]. All lesions were evaluated retrospectively with a commercial CAD system (Dynacad, version 2.1.7; Philips Healthcare). The software provided colour-coded maps of the DCE-MRI scans representing changes in signal intensity over time. We used the first post-contrast scan as the "early" image and the last (4th) post-contrast scan as the "delayed" image. The same two radiologists manually identified, with the help of the colour-coded map, a single voxel within each lesion that had the highest signal intensity in the "early" image for all 141 lesions [25] (Fig. 2a). The signal intensity of a voxel is obtained by averaging the signal of 9 neighbouring voxels in Dynacad, making this particular voxel to be in the centre of 3 × 3 voxels. Thus, the signal we obtained is processed through the noise reduction method. From this voxel, the initial enhancement rate (IER) and the signal enhancement ratio (SER) were calculated, where IER was defined as IER = $(SI_{early} - SI_{pre}) / SI_{pre}$ and SER was defined as SER = $(SI_{early} - SI_{pre}) / (SI_{delayed} - SI_{pre})$; SI denotes signal intensity of the manually identified voxel in the pre-contrast standard scan and in the "early" and "delayed" post-contrast standard scans (Fig. 2b). To evaluate an inter-reader agreement in the IER and SER from DCE-MRI, the IER and SER from DCE-MRI for each reader were analysed using the interclass correlation coefficient (ICC). Then, IER and SER from DCE-MRI were compared between benign and malignant lesions, and they were also compared to the results from EPT analysis.

Statistical analysis

The Mann-Whitney *U* test was used to comparing the patient age, FGT, lesion diameter, mean conductivity of EPT, the IER and SER of DCE-MRI between benign and malignant lesions. Fisher's exact test was used for comparing the lesion appearance (mass or non-mass) and presence/absence of clips between benign and malignant lesions. Spearman's correlation analysis was used for correlation of conductivity to patients' age and lesion diameter, Spearman's rank correlation analysis was used for correlation between conductivity and FGT, and Mann-Whitney *U* test was used for correlation between conductivity and the lesion appearance (mass or non-mass) and presence/absence of clips.

Interobserver reliability of the parameters from DCE-MRI was assessed using ICCs. An *r* of 1.0 was deemed to indicate perfect agreement; 0.81–0.99, almost perfect agreement; 0.61–0.80, substantial agreement; 0.41–0.60, moderate agreement; 0.21–0.40, fair agreement; 0.20 or less, slight agreement [29]. Multivariate linear regression analysis was performed to explore the relationship of various quantitative MR parameters (mean conductivity of

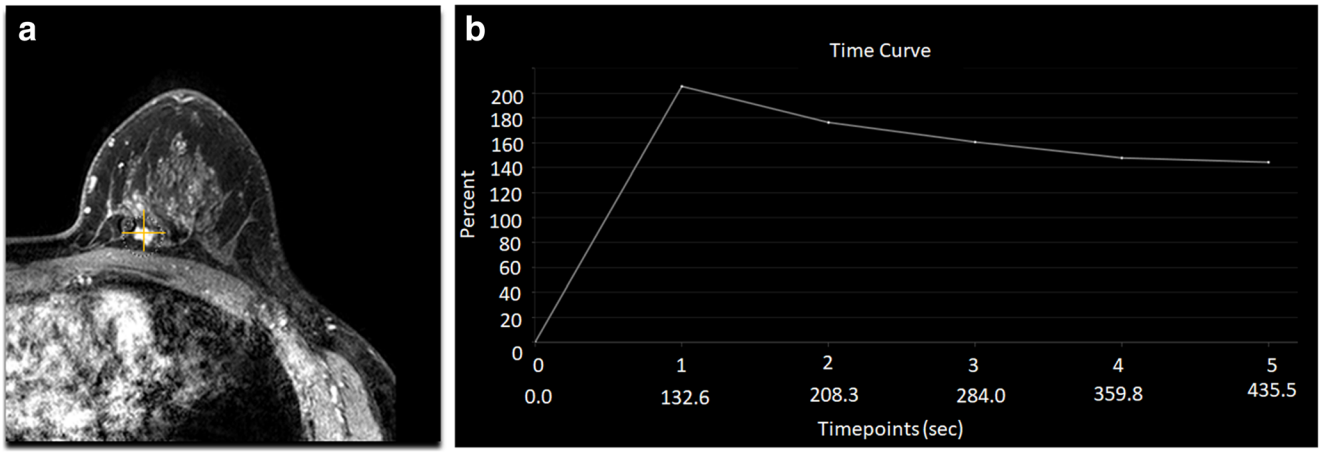

Fig. 2 Method to obtain kinetic parameter from dynamic contrast-enhanced (DCE) MRI. **a** A single voxel within the lesion that had the highest signal intensity in the "early" image was identified. **b** From this voxel, the initial enhancement rate (IER) and the signal enhancement ratio (SER) were calculated, where IER was defined as IER = $(SI_{early} - SI_{pre})/SI_{pre}$ and SER was defined as SER = $(SI_{early} - SI_{pre}) / (SI_{delayed} - SI_{pre})$; SI denotes signal intensity of the manually identified voxel in the pre-contrast standard scan and in the "early" and "delayed" post-contrast standard scans

EPT, the IER and SER of DCE-MRI) and their utility in differentiating between benign and malignant lesions.

The effectiveness of the parameters from EPT and DCE-MRI in differentiating between benign and malignant lesions was evaluated using receiver operating characteristic (ROC) analysis. The optimal thresholds for distinguishing malignant from benign lesions were chosen at the highest possible sensitivity and specificity (maximal Youden index defined as sensitivity plus specificity minus 1) on the ROC curves. Statistical analyses were performed using commercial software (JMP Pro 13; SAS Institute, Cary, NC, USA). A p value < 0.05 was considered significant.

Results

No statistically significant differences were found between the benign and malignant groups with respect to the amount of FGT and lesion appearance (mass or non-mass) ($p = 0.47$ and 0.80, respectively, Table 1); however, the malignant lesions showed a significantly higher age and larger lesion diameter than the benign lesions ($p = 0.011$ and $p < 0.0001$, respectively, Table 1). The frequency of lesions with clips were significantly higher in malignant lesion than in benign lesions ($p < 0.0001$, Table 1). There was no significant correlation between conductivity and age, FGT or lesion diameter ($r = -0.02$, 0.04 and 0.11, $p = 0.78$, 0.59 and 0.20, respectively [Table 2]). There was no significant difference in conductivity between mass and non-mass lesions ($p = 0.52$ [Table 2]). There was no significant difference in conductivity between lesions without and with clips ($p = 0.07$ [Table 2]). In evaluating the agreement between readers, ICCs for IER was 0.79, indicating substantial agreement, and ICC for SER was 0.81, indicating almost perfect agreement. In univariate analysis for EPT, mean conductivity of malignant lesions (1.14 ± 1.36 S/m) was significantly higher than that of benign lesions (0.14 ± 1.77 S/m) ($p < 0.0001$, Table 3, Figs. 3 and 4). For DCE-MRI, there was no significant difference between IER of malignant lesions (171 ± 64) and that of benign lesions (146 ± 75) ($p = 0.06$, Table 3). The SER of malignant lesions (1.04 ± 0.25) was significantly higher than that of benign lesions (0.77 ± 0.28) ($p < 0.0001$, Table 3).

In multivariate linear regression analysis, mean conductivity and SER were significantly associated with the differentiation between benign and malignant lesions ($p = 0.0027$, < 0.0001, respectively), while IER was not ($p = 0.21$) (Table 3).

Table 1 Patients' and lesions' characteristics

Variables	Benign ($n = 50$)	Malignant ($n = 91$)	p value
Age (years):			
median (range)	47 (23–76)	52 (28–76)	0.011
Amount of fibrograndular tissue (FGT) (n [%])			0.47
Almost entirely fat	1 (2)	1 (1)	
Scattered	19 (38)	31 (34)	
Heterogeneous	26 (52)	49 (54)	
Extreme	4 (8)	10 (11)	
Diameter (mm): median (range)	12 (5–91)	20 (7–107)	< 0.0001
The lesion appearance (n [%])			
Mass	44 (88)	78 (86)	0.80
Non-mass	6 (12)	13 (14)	
Presence/absence of clips (n [%])			
Without clips	36 (72)	10 (11)	< 0.0001
With clips	14 (28)	81 (89)	

Table 2 Relationship between conductivity and patients' and lesions' characteristics

Variables	Coefficients	*p*
Age (years)	-0.02[a]	0.78
FGT (almost entirely fat, scattered, heterogeneous, extreme)	0.04[b]	0.59
Diameter (mm)	0.11[a]	0.20
The lesion appearance (mass, non-mass)	NA[c]	0.52
Presence/absence of clips (without clips [$n = 46$], with clips [$n = 95$])	NA[c]	0.07

FGT fibrograndular tissue

[a] Spearman's correlation coefficient

[b] Spearman's rank correlation coefficient

[c] Mann-Whitney *U* test

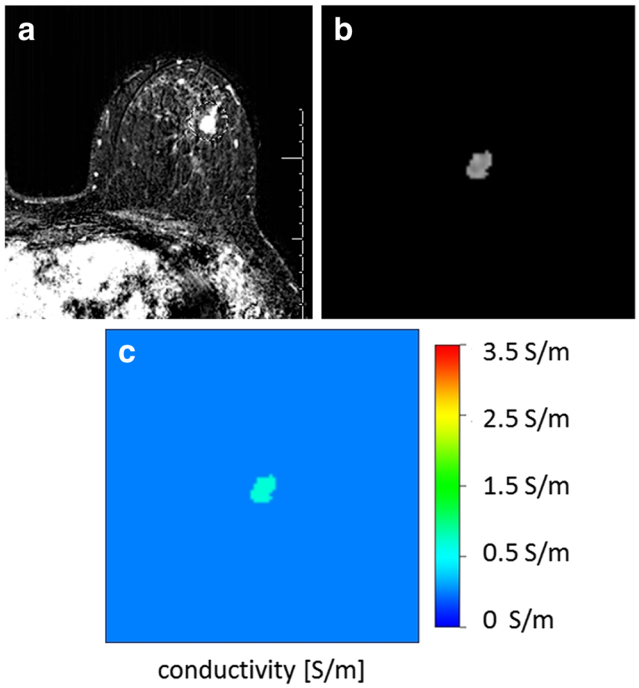

Fig. 3 A 52-year-old woman diagnosed with sclerosing adenosis by percutaneous biopsy. **a** Axial dynamic contrast-enhanced MR image obtained in early phase shows a mass lesion in the left breast. **b** The phase image obtained from 3D TSE shows a lesion with the binary mask. **c** Conductivity map shows the conductivity of the lesion is 0.66 S/m, lower than the cut-off value of 0.88 S/m, indicating the lesion as benign

ROC analysis revealed that the area under the curve (AUC) of mean conductivity, the IER and SER were 0.71 (Fig. 5a), 0.59 and 0.80 (Fig. 5b), respectively (Table 3). For EPT, the ROC curve analysis showed that the most effective threshold for the mean conductivity to discriminate malignant from benign lesions was 0.88 S/m, and by using this threshold, the sensitivity, specificity, positive predictive value and negative predictive value were 64%, 76%, 83%, and 54%, respectively (Fig. 5a). For DCE-MRI, the ROC curve analysis showed that the most effective threshold for the SER to discriminate malignant from benign lesions was 0.92, and by using this threshold, the sensitivity, specificity, positive predictive value and negative predictive value were 85%, 72%, 84%, and 73%, respectively (Fig. 5b).

There was no significant difference between AUC of the mean conductivity and the SER ($p = 0.15$).

Discussion

In this study, images acquired with two methods, EPT and DCE-MRI, are manifestations of two different underlying mechanisms. While DCE-MRI demonstrates the amount of leakage of contrast medium into the extracellular space; EPT demonstrates metabolic changes in the tissue, in which TSC is the most influential factor for an elevation of conductivity in tumours [14]. In fact, Zaric et al [30] reported that TSC in malignant lesions was significantly higher than that in benign lesions using sodium-23 (^{23}Na) MRI in a 7-T system with a small number of subjects (5 benign and 15 malignant breast lesions). Although it might be interesting to know the combined diagnostic ability of EPT and DCE-MRI, it was not evaluated as the purpose of this study was to compare EPT to DCE-MRI with respect to the ability to differentiate between benign and malignant lesions. On the other hand, there was no significant difference between benign and malignant lesions with IER. The reason for no significant difference in IER may be due to the relatively small number of cases and/or the variety of pathological entities.

Table 3 Comparison of parameters from EPT and DCE-MRI between malignant and benign lesions

Variables	Benign ($n = 50$)	Malignant ($n = 91$)	*p* value (univariate)	*p* value (multivariate)	AUC
EPT					
The mean conductivity	0.14 ± 1.77	1.14 ± 1.36	< 0.0001	0.0027	0.71
DCE-MRI					
IER	146 ± 75	171 ± 64	0.06	0.21	0.59
SER	0.77 ± 0.28	1.04 ± 0.25	< 0.0001	< 0.0001	0.80

IER initial enhancement rate, *SER* signal enhancement ratio

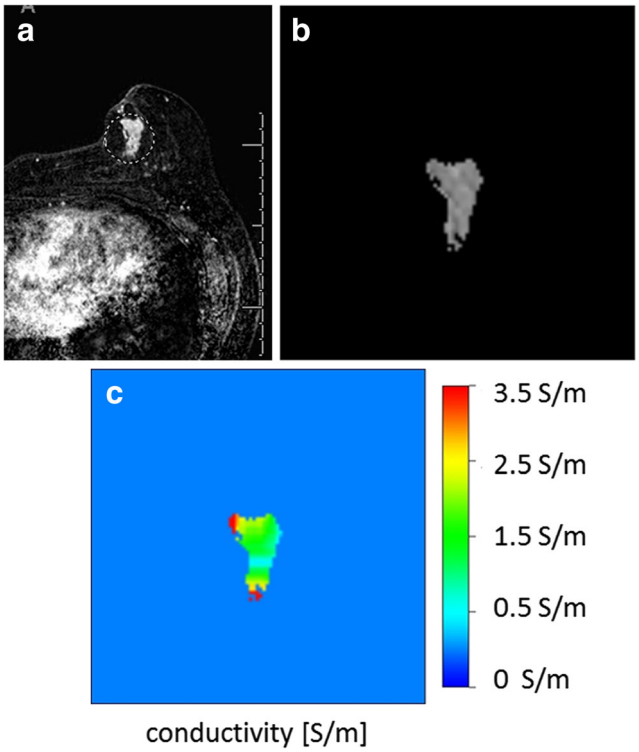

Fig. 4 A 67-year-old woman diagnosed with invasive ductal carcinoma by percutaneous biopsy. **a** Axial dynamic contrast-enhanced MR image obtained in early phase shows a mass lesion in the left breast. **b** The phase image obtained from 3D TSE shows the lesion with the binary mask. **c** Conductivity map shows the conductivity of the lesion is 2.02 S/m, higher than the cut-off value of 0.88 S/m, indicating the lesion as malignant

Electrical conductivity is denoted as σ in units of Siemens/metre (S/m), and in vivo and in vitro experiments using electrical impedance tomography (EIT) with a needle electrode or scan probe have been conducted [31–33]. The conductivities of malignant breast lesions are typically in the range of 0.8-1.4 S/m, while those of normal breast tissue are between 0.1 and 0.2 S/m [33, 34]. However, the EIT method had its limitations, including invasive insertion of needle electrode and low spatial resolution images obtained from outside of the body.

The capability of MRI to obtain the conductivity of tissue in a non-invasive manner was first suggested by Haacke et al [35]. Several studies showed significantly higher conductivity in malignant tumours than in normal tissues in the brain and the breast [20, 22, 23]. However, there has only been one study that showed differing conductivity between benign and malignant lesions to our knowledge [23]. In this current study, we compared the conductivity between benign and malignant lesions, using a larger sample size than that of Shin et al [23], thus reinforcing the results that the mean conductivity of EPT might be a novel non-contrast approach to differentiate benign from malignant lesions. Furthermore, our results showed that the mean conductivity of malignant lesions (1.14 ± 1.36 S/m) fell within the reported range from 0.8 to1.4 S/m, and we revealed that the mean conductivity of benign lesions was 0.14 ± 1.77 S/m.

One of the advantages of EPT is that it does not require special MRI sequences to obtain the conductivity. The imaging sequence employed to obtain conductivity maps was a routine non-contrast clinical protocol, 3D TSE (T2 VISTA), and the acquisition time of this protocol was comparable to that of DCE-MRI; 5 min 10 s for 3D TSE versus 6 min 56 s for DCE-MRI. Another advantage of EPT is that it does not require contrast medium. However, there are issues to be resolved as the current methods shown here depend on DCE-MRI to segment a lesion for conductivity. Future research will focus on developing a conductivity map of the whole breast from a non-contrast technique; thus, enabling EPT to be a potential option as a screening study due to its non-invasive, non-contrast features.

In this study, minimal lesion diameter of 7 voxels (5.6 × 5.6 × 11.2 mm^3) was necessary for the calculation of conductivity, and we excluded 12 out of 133 patients as a result of this requirement. Higher spatial resolution and a modified EPT

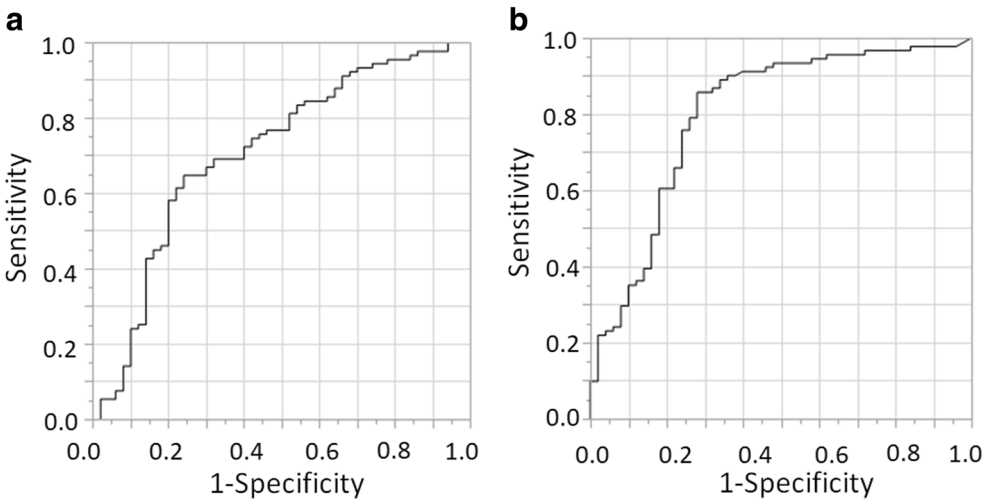

Fig. 5 Graph of the receiver operating curve (ROC) for the mean conductivity of EPT (**a**) and SER of DCE-MRI (**b**) for differentiating benign and malignant lesions shows that the area under the ROC curve is 0.71 and 0.80, respectively

algorithm [36] would enable the reconstruction of smaller lesions in the future.

This study has several limitations. First, this is a retrospective study with no test data set and the number of lesions of each subtype in benign and malignant groups was still small. Second, MRI was performed after biopsy and placement of clips in 80 lesions of malignant and 14 lesions of benign pathology results. The conductivity might be sensitive to haemorrhage from biopsy or metallic clips, and further studies excluding these factors should be performed. Third, we did not compare the mean conductivity with the parameters of diffusion weighted images (DWI), which is another conventional non-contrast sequence. Kim et al [37] showed negative correlation between conductivity and apparent diffusion coefficient from DWI in breast cancer. Although it is currently out of the scope of our study, comparing EPT to DWI might be of interest in the future as each method might reflect a different state of the tissue. Fourth, the diameter of malignant lesions was significantly larger than benign lesions. The method to obtain the conductivity is based on the assessment of surrounding voxels, potentially making its value to be dependent on the size of the lesion. However, there was no significant relationship between the conductivity and the diameter of the lesions in our study (Table 2). Further evaluation with size-matched subjects might be necessary to confirm the results. Fifth, we did not evaluate whether there was a significant difference in conductivity between benign and malignant non-mass lesions, because there were not enough non-mass lesions to have meaningful results. Further study with non-mass lesions might be necessary in the future.

In conclusion, the mean conductivity was significantly different between benign and malignant breast lesions as well as kinetic parameter or SER from DCE-MRI for lesions above a certain size. With larger scale studies and refinement of the EPT algorithm, this technique may be a potential option as a screening study due to its non-invasive, non-contrast features.

Acknowledgements This research was partly supported by Philips Healthcare. The authors thank Sharon Harris in the University of Chicago, for her kind support. The authors thank Yumi Fujimoto, Shomo Chou in Tohoku University for their kind support.

Funding The authors state that this work has not received any funding.

Compliance with ethical standards

Guarantor The scientific guarantor of this publication is Hiroyuki Abe.

Conflict of interest The authors (Naoko Mori, Keiko Tsuchiya, Deepa Sheth, Shunji Mugikura, Kei Takase and Hiroyuki Abe) of this manuscript declare no relationships with any companies, whose products or services may be related to the subject matter of the article.

Ulrich Katscher is an employee of Philips Technologie GmbH, Research Laboratories.

Statistics and biometry No complex statistical methods were necessary for this paper.

Informed consent Written informed consent was waived by the Institutional Review Board.

Ethical approval Institutional review board approval was obtained.

Methodology
- Retrospective
- Diagnostic or prognostic study
- Performed at one institution

References

1. Kriege M, Brekelmans CT, Boetes C et al (2004) Efficacy of MRI and mammography for breast-cancer screening in women with a familial or genetic predisposition. N Engl J Med 351:427–437
2. Warner E, Messersmith H, Causer P, Eisen A, Shumak R, Plewes D (2008) Systematic review: using magnetic resonance imaging to screen women at high risk for breast cancer. Ann Intern Med 148: 671–679
3. Kuhl CK, Schrading S, Leutner CC et al (2005) Mammography, breast ultrasound, and magnetic resonance imaging for surveillance of women at high familial risk for breast cancer. J Clin Oncol 23: 8469–8476
4. Warner E, Plewes DB, Hill KA et al (2004) Surveillance of BRCA1 and BRCA2 mutation carriers with magnetic resonance imaging, ultrasound, mammography, and clinical breast examination. JAMA 292:1317–1325
5. Lehman CD, Blume JD, Weatherall P et al (2005) Screening women at high risk for breast cancer with mammography and magnetic resonance imaging. Cancer 103:1898–1905. https://doi.org/10.1002/cncr.20971
6. American College of Radiology (2013) Breast imaging reporting and data system (BI-RADS), 5th edn. American College of Radiology, Reston
7. Brasch RC, Weinmann H-J, Wesbey GE (1984) Contrast-enhanced NMR imaging: animal studies using gadolinium-DTPA complex. AJR 142:625–630
8. Revel D, Brasch RC, Paajanen H et al (1986) Gd-DTPA contrast enhancement and tissue differentiation in MR imaging of experimental breast carcinoma. Radiology 158:319–323
9. Heuser LS, Miller FN (1986) Differential macromolecular leakage from the vasculature of tumors. Cancer 57:461–464
10. Wikström MG, Moseley ME, White DL et al (1989) Contrast-enhanced MRI of tumors. Comparison of Gd-DTPA and a macromolecular agent. Invest Radiol 24:609–615
11. Kanda T, Ishii K, Kawaguchi H, Kitajima K, Takenaka D (2013) High signal intensity in the dentate nucleus and globus pallidus on unenhanced T1-weighted MR images: relationship with increasing cumulative dose of a gadolinium-based contrast material. Radiology 270:834–841
12. McDonald RJ, McDonald JS, Kallmes DF et al (2015) Intracranial gadolinium deposition after contrast-enhanced MR imaging. Radiology 275:772–782
13. Katscher U, Kim DH, Seo JK (2013) Recent progress and future challenges in MR electric properties tomography. Comput Math Methods Med 2013:1–11
14. Ouwerkerk R, Jacobs MA, Macura KJ et al (2007) Elevated tissue sodium concentration in malignant breast lesions detected with non-invasive 23Na MRI. Breast Cancer Res Treat 106:151–160

15. Cameron IL, Smith NK, Pool TB, Sparks RL (1980) Intracellular concentration of sodium and other elements as related to mitogenesis and oncogenesis in vivo. Cancer Res 40:1493–1500
16. van Lier A, de Bruin P, Aussenhofer S et al (2013) ^{23}Na-MRI and EPT: are sodium concentration and electrical conductivity at 298 MHz (7 T) related? Proc Intl Soc Mag Reson Med 21, Salt Palace Convention Center, Salt Lake City
17. Lagarde AE, Pouysségur JM (1986) The Na+:H+ antiport in cancer. Cancer Biochem Biophys 9:1–14
18. Ouwerkerk R, Bleich KB, Gillen JS, Pomper MG, Bottomley PA et al (2003) Tissue sodium concentration in human brain tumors as measured with 23Na MR imaging. Radiology 227:529–537
19. Huhndorf M, Stehning C, Rohr A, Helle M, Katscher U, Jansen O (2013) Systematic brain tumor conductivity study with optimized EPT Sequence and reconstruction algorithm. Proc 21st Intl Soc Mag Reson Med, Salt Palace Convention Center, Salt Lake City, 20-26 April 2013
20. Voigt T, Väterlein O, Stehning C, Katscher U, Fiehler J (2011) In vivo glioma characterization using MR conductivity imaging. Proc Int Soc Magn Reson Med 19, Palais des congrès de Montréal, Montréal
21. van Lier AL, Hoogduin JM, Polders DL (2011) Electrical conductivity imaging of brain tumours. Proc 19th Sci Meet Int Soc Magn Reson Med, Palais des congrès de Montréal, Montréal, 7-13 May 2011
22. Tha KK, Katscher U, Yamaguchi S et al (2018) Noninvasive electrical conductivity measurement by MRI: a test of its validity and the electrical conductivity characteristics of glioma. Eur Radiol 28: 348–355
23. Shin J, Kim MJ, Lee J et al (2015) Initial study on in vivo conductivity mapping of breast cancer using MRI: in vivo conductivity mapping of breast cancer. J Magn Reson Imaging 42:371–378
24. Kim SY, Shin J, Kim DH et al (2016) Correlation between conductivity and prognostic factors in invasive breast cancer using magnetic resonance electric properties tomography (MREPT). Eur Radiol 26:2317–2326
25. Abe H, Mori N, Tsuchiya K et al (2016) Kinetic analysis of benign and malignant breast lesions with ultrafast dynamic contrast-enhanced MRI: comparison with standard kinetic assessment. AJR Am J Roentgenol 207:1159–1166
26. Katscher U, Voigt T, Findeklee C, Vernickel P, Nehrke K, Dössel O (2009) Determination of electric conductivity and local SAR via B1 mapping. IEEE Trans Med Imaging 28:1365–1374
27. Sujji GE, Lakshmi YVS, Jiji GW (2013) MRI brain image segmentation based on thresholding. Int J Adv Comput Res 3:97–101
28. Katscher U, van den Berg CAT (2017) Electric properties tomography: biochemical, physical and technical background, evaluation and clinical applications. NMR Biomed 30:e3729. https://doi.org/10.1002/nbm.3729
29. Landis JR, Koch GG (1977) The measurement of observer agreement for categorical data. Biometrics 33:159–174
30. Zaric O, Pinker K, Zbyn S et al (2016) Quantitative sodium MR imaging at 7 T: initial results and comparison with diffusion-weighted imaging in patients with breast tumors. Radiology 280: 39–48
31. Zou Y, Guo Z (2003) A review of electrical impedance techniques for breast cancer detection. Med Eng Phys 25:79–90
32. Poplack SP, Tosteson TD, Wells WA et al (2007) Electromagnetic breast imaging: results of a pilot study in women with abnormal mammograms. Radiology 243:350–359
33. Joines WT, Zhang Y, Li C, Jirtle RL (1994) The measured electrical properties of normal and malignant human tissues from 50 to 900 MHz. Med Phys 21:547–550
34. Surowiec AJ, Stuchly SS, Barr JR, Swarup A (1988) Dielectric properties of breast carcinoma and the surrounding tissues. IEEE Trans Biomed Eng 35:257–263
35. Haacke E, Petropoulos LS, Nilges EW, Wu D (1991) Extraction of conductivity and permittivity using MRI. Phys Med Biol 38:723–741
36. Lee J, Choi N, Seo JK, Kim DH (2017) Magnetic resonance electrical properties tomography for small anomalies using boundary conditions: a simulation study. Med Phys 44:4773–4785
37. Kim SY, Shin J, Kim DH et al (2018) Correlation between electrical conductivity and apparent diffusion coefficient in breast cancer: effect of necrosis on magnetic resonance imaging. Eur Radiol 28: 3204–3214